receiving data from Galileo. In 2002, when the Cassini spacecraft flies by Jupiter *en route* to Saturn, we will get the first compositional measurements of the dust grains, which will provide more clues to their origin[12]. □

Received 22 January; accepted 2 April 1996.

1. Grün, E. *et al. Nature* **362,** 428–430 (1993).
2. Baguhl, M., Grün, E., Linkert, G., Linkert, D. & Siddique, N. *Planet. Space Sci.* **41,** 1085–1098 (1993).
3. Grün, E. *et al. Geophys. Res. Lett.* **21,** 1035–1038 (1994).
4. Hamilton, D. P. & Burns, J. A. *Nature* **364,** 695–699 (1993).
5. Horányi, M., Morfill, G. E. & Grün, E. *Nature* **363,** 144–146 (1993); *J. geophys. Res.* **98,** 21245–21251 (1993).
6. Grün, E. *et al. Space Sci. Rev.* **60,** 317–340 (1992).
7. Grün, E. *et al. Astr. Astrophys. Suppl.* **92,** 411–423 (1992).
8. Grün, E. *et al. Planet. Space Sci.* **43,** 941–951 (1995).
9. Zook, H. A. *et al.* in *Physics, Chemistry, and Dynamics of Interplanetary Dust* (eds Gustafson, B. A. S. & Hanner, M. S.) (Conf. Ser., Astr. Soc. Pacific, Provo, UT, in the press).
10. Kivelson, M. G., Khurana, K. K., Means, J. D., Russell, C. T. & Snare, R. C. *Space Sci. Rev.* **60,** 357–384 (1992).
11. Johnson, T. V., Morfill, G. E. & Grün, E. *Geophys. Res. Lett.* **7,** 305–308 (1980).
12. Srama, R., Grün, E. and the Cassini Dust Science Team in *Physics, Chemistry, and Dynamics of Interplanetary Dust* (eds Gustafson, B. A. S. & Hanner, M. S.) (Conf. Ser., Astr. Soc. Pacific, Provo, UT, in the press).
13. Collins, S. A. *J. geophys. Res.* **86,** 8621–8626 (1981).
14. Baguhl, M. *et al. Space Sci. Rev.* **72,** 471–476 (1995).

ACKNOWLEDGEMENTS. We thank the Galileo operations team at JPL for their efficient cooperation and especially for the special campaigns that they provided. This work was supported by DARA.

Direct observation of a surface charge density wave

Joseph M. Carpinelli*, Hanno H. Weitering*, E. Ward Plummer* & Roland Stumpf†

* Department of Physics and Astronomy, The University of Tennessee, Knoxville, Tennessee 37996, USA, and Solid State Division, Oak Ridge National Laboratory, Oak Ridge, Tennessee 37831, USA
† Sandia National Laboratory, Albuquerque, New Mexico 87185, USA

A CHARGE density wave (CDW) is a periodic symmetry-lowering redistribution of charge within a material, accompanied by a rearrangement of electronic bands (such that the total electronic energy is decreased) and usually a small periodic lattice distortion[1,2]. This phenomenon is most commonly observed in crystals of reduced symmetry, such as quasi-two-dimensional[3] or quasi-one-dimensional[4] materials. In principle, the reduction of symmetry associated with surfaces and interfaces might also facilitate the formation of CDWs; although there is some indirect evidence for surface charge density waves[5–12,14], none has been observed directly. Here we report the observation and characterization of a reversible, temperature-induced CDW localized at the lead-coated (111) surface of a germanium crystal. The formation of this new phase is accompanied by significant periodic valence-charge redistribution, a pronounced lattice distortion and a metal–nonmetal transition. Theoretical calculations confirm that electron–phonon coupling drives the transition to the CDW, but it appears that some other factor—probably electron–electron correlations—is responsible for the ground-state stability of this phase.

Pb/Ge(111)-α consists of 1/3 monolayer of equivalent lead adatoms spaced ~7 Å apart in a hexagonal array of T_4 sites atop the bulk-truncated germanium lattice, forming the $(\sqrt{3} \times \sqrt{3})R30^\circ$ arrangement shown in Fig. 1. Clean, well ordered germanium (111) surfaces were first prepared in ultrahigh vacuum, followed by a room-temperature lead dose and subsequent anneal (at ~250 °C) to produce α-phase[15–19]. Coverage was monitored with both low-energy electron diffraction (LEED) and Auger electron spectroscopy. In practice, some Ge adatom defects were always present in the overlayer.

We employed three experimental surface analysis techniques to characterize this thin film. LEED was used to determine the symmetry of the surface atomic lattice. Inelastic electron scattering (electron energy-loss spectroscopy (EELS)) was used to probe the excitation spectra of our interface. Scanning tunnelling microscopy (STM) was used to image the spatial variations in the surface charge density with atomic resolution[20].

We present first our results acquired at room temperature, where all previous investigations were performed[15–19,21]. LEED data (Fig. 2*a*) include several sharp diffraction spots, characteristic of the $(\sqrt{3} \times \sqrt{3})R30^\circ$ surface symmetry displayed in Fig. 1. EELS data (Fig. 2*a*) indicate that the room-temperature α-phase is metallic. This result is consistent with simple electron counting, where (based on the Pauli principle) two electrons from each unit cell sequentially populate the electronic bands (starting from low energy). In any geometry with an odd number of electrons per unit cell, the uppermost occupied band will be only partially filled, resulting in a metallic structure. The $(\sqrt{3} \times \sqrt{3})R30^\circ$ surface unit cell contains one lead atom (with a valency of four) and three outer layer germanium atoms (each with one unpaired electron), totalling seven valence electrons in all, and is therefore expected to be metallic. Figure 3*a* presents room-temperature STM data acquired in the same scan but at different bias voltages. In both the filled state and empty state, a hexagonal array of identical protrusions can be seen. The results of previous experiments[18] and computer simulations[19] indicate that each protrusion imaged is a lead adatom.

As the sample temperature is lowered, properties of the α-phase exhibit a dramatic change. For surfaces with a low enough defect density, the low-temperature LEED pattern now shows the presence of extra spots (Fig. 2*b*), characteristic of a new (3 × 3) symmetry. This transition in structure is gradual and reversible, with an onset near −20 °C. EELS data of the low temperature α-phase are likewise very different from their room-temperature counterparts. There is no continuum of low energy losses; instead, a discrete loss onset can be seen, indicating a semiconducting interface. The inset of Fig. 2*b* shows similar data for a non-zero parallel momentum transfer (angle of reflection ≠ angle of incidence) indicating more clearly the onset value. Whereas the room temperature α-phase is metallic, our observations indicate that a small band gap ($E_g \leqslant 0.065$ V at 100 K) evolves as tempera-

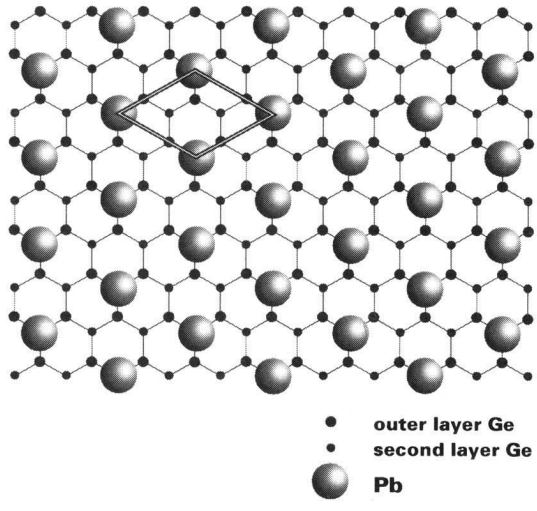

FIG. 1 Ball model of the α-phase of Pb/Ge(111); coverage is 1/3 monolayer. Lead adatoms are 7.0 Å apart on T_4 sites atop the bulk truncated germanium lattice. The indicated unit cell shows the interface's $(\sqrt{3} \times \sqrt{3})R30^\circ$ symmetry (relative to the bulk truncated (1 × 1) symmetry).

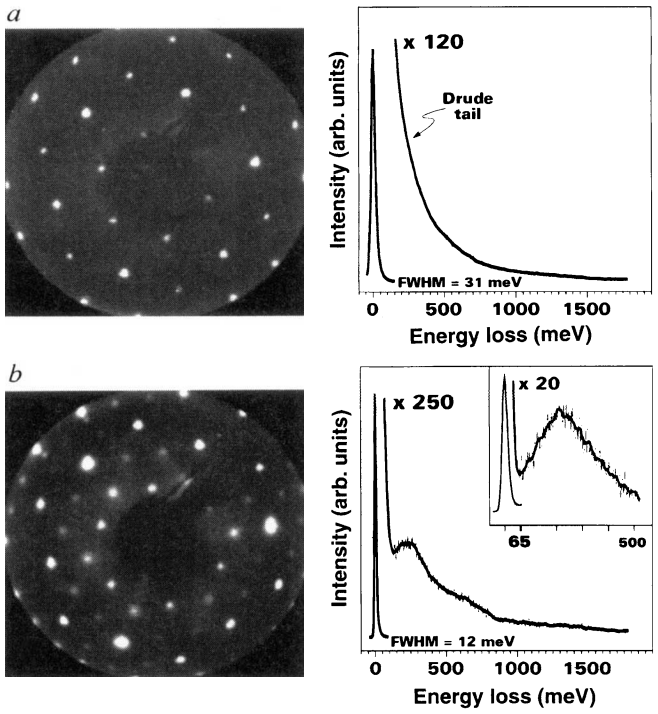

FIG. 2 Room-temperature (*a*) and low-temperature (*b*; $T \approx 100$ K) LEED (left) and EELS (right) data from the α-phase; beam energy for LEED was 48.6 eV. In LEED, the change in symmetry from the room-temperature $(\sqrt{3} \times \sqrt{3})R30^\circ$ structure to the low-temperature (3×3) structure is highlighted by the emergence of many new diffraction maxima. At room temperature, EELS indicates that α-phase is metallic by (1) the presence of a broad, slowly decreasing Drude tail, produced when electrons at the Fermi level are excited into the adjacent continuum of empty states, and (2) the absence of a discrete energy loss onset. The discrete onset in the low-temperature spectrum, created when electrons are excited with minimum excitation energy into the unoccupied bands, indicates a surface band gap. The energy onset of such a loss spectrum corresponds to the gap magnitude E_g. Inset, off-specular data (non-zero parallel momentum transfer) indicating that the ground state band gap is no more than 65 meV.

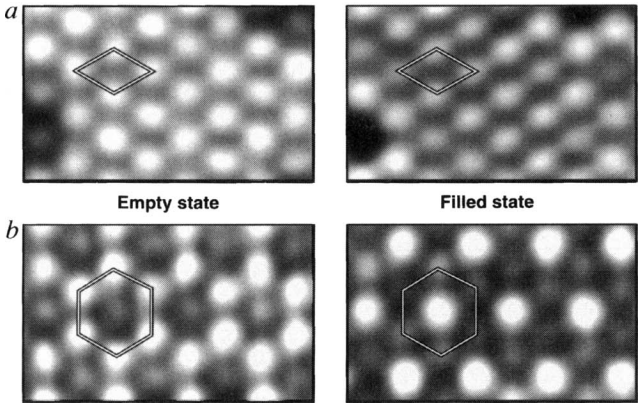

FIG. 3 Room-temperature (*a*) and low-temperature (*b*; $T \approx 60$ K) STM data from the α-phase. Empty- and filled-state images were acquired with sample bias $V_s = +1$ V (electrons tunnelling out from the sample) and -1 V (electrons tunnelling into the sample) respectively. Their registry is assured, that is, each point in the empty-state image is produced from the same real space coordinate as the corresponding point in the filled-state image. At room-temperature, each lead adatom appears identical, whereas at low temperature, a honeycomb-pattern charge rearrangement is evident. Repeat units are identified in each image.

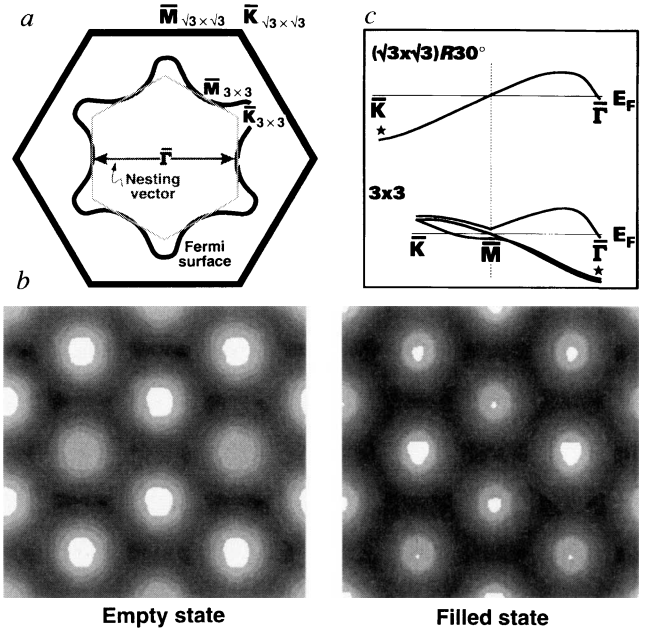

FIG. 4 Calculations of electronic structure were performed for several supercells with various *k*-point samplings. During the calculations of the low-temperature phase, the outermost germanium layers and the lead layer were allowed to relax. *a*, The wavy black line inside the outer hexagon (first Brillouin zone) is a curve drawn through calculated Fermi surface points for the $(\sqrt{3} \times \sqrt{3})R30^\circ$ structure. The illustrated nesting vector is $1/\sqrt{3}$ the length of a reciprocal lattice vector, matching the new ground-state symmetry of (3×3); the new Brillouin zone is indicated in grey. *b*, Calculated contours of constant integrated density of states (between E_F and $+1$ or -1 V) for the fully relaxed structure, showing the observed (3×3) symmetry and honeycomb-pattern charge rearrangement. *c*, Calculated band structure along high-symmetry directions for both the $(\sqrt{3} \times \sqrt{3})R30^\circ$ and (3×3) structures. Although the former structure is metallic with a single band crossing midway between the zone centre ($\bar{\Gamma}$) and the zone boundary ($\bar{K}$), a small gap opens between two bands at this location (the new $\bar{M}$ point) in the SCDW phase, while a third crosses E_F. This gap is localized in a small area of the surface Brillouin zone and, therefore, the calculated outer layer density of states near E_F shows practically no change between the room-temperature and low-temperature structures. Note that the two filled bands from $\bar{\Gamma}$ to $\bar{M}$ in the (3×3) structure are roughly those expected from folding back the $(\sqrt{3} \times \sqrt{3})R30^\circ$ band approaching $\bar{K}$ (stars denote equivalent *k*-space locations). For both structures, valence bands disperse about 0.6 V.

ture is lowered. Our EELS study suggests that this electronic transition also occurs gradually and reversibly, but at a slightly lower onset temperature than the structural transition.

It is the change in STM imaging at low temperatures, however, that elucidates the nature of the observed transition. Low-temperature filled- and empty-state images of α-phase are shown in Fig. 3*b*. Unlike the room-temperature results, Pb adatoms no longer appear equivalent, and the same (3×3) symmetry found in low-temperature LEED data can be seen. This is not the result of a rippled topography. Rather, it reflects the sensitivity of the STM technique to the spatial profile of occupied (filled-state image) and unoccupied (empty-state image) electronic states. One out of three Pb adatoms now possess an enhanced relative concentration of filled states (and appears brighter in the filled-state image). This same atom also possesses a diminished relative concentration of empty states (and appears darker in the empty-state image). The result is a honeycomb-patterned charge superstructure commensurate with the underlying lattice. As the sample temperature increases, this new charge superstructure gradually subsides and the sample returns to the equivalent adatom configuration of room temperature.

What we observe experimentally is now clear. On decreasing temperature, the Pb/Ge(111)-α system forms a commensurate

surface charge density wave (SCDW) independent of any bulk phenomena. This transition occurs gradually and reversibly with an onset just below room temperature. As with many examples of bulk CDWs, this surface rearrangement of valence charge incorporates a structural distortion. Comparison of our LEED data to that of other systems suggests the lead atom plane is significantly rumpled at low temperature, probably of the order of ~0.2 Å. The measured value of the SCDW band gap, ~0.065 V, corresponds well with the observed critical temperature, ~−20 °C, via the mean-field CDW relationship, $E_g = 3.53 K_B T_c$ (ref. 22). The value of the tiny SCDW band gap measured by EELS could not be reliably verified using STM (as is generally possible[23]) in our case owing to signal-to-noise problems at the Fermi energy (E_F).

The only major inconsistency with the simple SCDW picture results form electron counting. The new low-temperature (3 × 3) unit cell is three times as large as the room-temperature $(\sqrt{3} \times \sqrt{3})R30°$ cell, containing three lead and nine germanium atoms and, therefore, 21 valence electrons. This is again a sufficient condition for metallicity, in stark contradiction to the semiconducting ground state inferred from the EELS data.

In an attempt to identify the driving force for stabilization of a SCDW, we performed first-principle density functional calculations[24] for this system using the local density approximation. The calculations confirm that the room-temperature phase should be metallic with a half-filled band of surface states positioned in the gap region of the germanium substrate. In Fig. 4*a*, the wavy black line inside the $(\sqrt{3} \times \sqrt{3})R30°$ surface Brillouin zone (the outer hexagon) depicts the shape and location of the calculated two-dimensional Fermi surface. A vector of constant momentum transfer connecting parallel segments of Fermi surface, called a nesting vector, is identified. The electronic response function of a nested Fermi surface is strongly peaked at twice the Fermi wavevector ($2k_F$), which facilitates enhanced electronic screening of phonons (quantized lattice vibrations) with momentum $2k_F$. This screening results in a soft phonon at $2k_F$, called a Kohn anomaly. If the nesting (and hence the screening) is strong enough, a static lattice distortion can occur, incorporating the symmetry of the nesting vector. As seen in Fig. 4*a*, the predicted nesting vectors match the symmetry of the observed (3 × 3) ground state (inner hexagon, Fig. 4*a*). Therefore, theory predicts that Fermi-surface nesting, or more generally electron–phonon coupling, drives this transition.

When not constrained in our calculation, lead and surface germanium atoms rearrange themselves spontaneously in a (3 × 3) structure, reducing the total energy by about 0.020 eV per $(\sqrt{3} \times \sqrt{3})R30°$ unit cell. The corrugation of the lead adlayer is ~0.05 Å. Two simulated STM images for this structure (Fig. 4*b*) show remarkable qualitative agreement with the experimental data. Figure 4*c* shows the calculated band structure near the Fermi energy for both the $(\sqrt{3} \times \sqrt{3})R30°$ and (3 × 3) structures. At room-temperature, a single half-filled band (with strong lead p_z character) crosses the Fermi energy. Owing to the reduced symmetry, three bands exist in this region at low temperature: one crosses the Fermi energy (metallic) as before, but the other two show the effect of the new SCDW periodicity, opening up a small gap at the new (3 × 3) zone boundary (M̄). However, problems still exist. First, the calculated distortion of the lead atoms is not large enough to account for the intensity of the fractional-order LEED spots. Second, and most importantly, the theoretical (3 × 3) surface is metallic, contrary to our EELS data. But the apparent shortcomings of theory might in fact indicate the true nature of the ground state. We infer that electron–electron interactions (not properly accounted for in the local density approximation) result in larger-than-predicted lattice displacements, as well as the formation of a surface band gap (a Mott insulator) which further stabilizes the low-temperature phase. This is a reasonable inference, as calculated charge density plots for Pb/Ge(111) indicate the states involved with Fermi surface nesting are localized, a necessary precursor to the onset of significant correlation effects. The role of electron correlation in CDW formation and stability was first discussed by Overhauser[25].

Although most of the bulk quasi-two-dimensional CDWs are driven purely by a bond reorganization, our SCDW is reminiscent of that for the layered compound 1T-TaS_2 (refs 26–28). In this system, lowering sample temperature initiates a reversible transition in the CDW phase from an incommensurate structure to a commensurate one, accompanied by the sharp evolution of a pseudo-gap (again contrary to electron counting). But in contrast to Pb/Ge(111)-α, TaS_2 Mott localization has been considered only an accidental consequence of the CDW distortion and was not considered responsible for its stability.

Although other proposed examples of CDWs at surfaces exist, Pb/Ge(111) is thus far unique. For example, surfaces of the layered transition metal dichalcogenides[28] (including TaS_2) possess a charge superstructure, but only as the termination of bulk CDWs. The reconstruction of semiconductor surfaces on cleaving in vacuum is sometimes referred to as a CDW[1,2], but these transitions are irreversible in the experimentally accessible temperature range, involve large structural distortions, and can be accounted for by covalent bond rearrangement. On other surfaces including W(100) and Mo(100) (refs 5–11), and alkali-metal covered Cu(111) (ref. 12), CDWs have been speculated to account for certain experimental data, but have not been directly observed. A Peierls distortion[13], the one-dimensional analogue of a CDW, has likewise been proposed to explain anomalous observations of Tl/Cu(110) (ref. 14).

It is likely that other unmistakable SCDWs will be found within the wealth of known metal–semiconductor interfaces. For example, aluminum, indium, gallium, lead and tin all produce T_4 adatom α-type structures on Si(111) at room temperature. A determination of which systems undergo the SCDW transformation will lend further insight into the physical processes responsible for this phenomenon. It might even be possible to 'engineer' the Fermi surface by co-deposition of different adatom species, producing a range of both commensurate and incommensurate low-temperature structures. □

Received 23 January; accepted 25 April 1996.

1. Tosatti, E. *Electronic Surface and Interface States on Metallic Systems* (eds Bertel, E. and Donath, M.) (World Scientific, Singapore, 1995).
2. Tosatti, E. *Festkorperprobeleme* **15,** 113–147 (1975).
3. Wilson, J. A., DiSalvo, F. J. & Mahajan, S. *Phys. Rev. Lett.* **32,** 882–885 (1974).
4. Grüner, G. *Density Waves in Solids* (Addison Wesley, Reading, MA, 1994).
5. Felter, T. E., Barker, R. A. & Estrup, P. J. *Phys. Rev. Lett.* **38,** 1138–1141 (1977).
6. Debe, M. K. & King, D. A. *J. Phys. C: Solid St. Phys.* **10,** L303–L308 (1977).
7. Wang, X. W. & Webber, W. *Phys. Rev. Lett.* **58,** 1452–1455 (1987).
8. Tosatti, E. *Solid St. Commun.* **25,** 637–640 (1978).
9. Wang, C. Z., Fasolino, A. & Tosatti, E. *Phys. Rev.* B**37,** 2116–2122 (1988).
10. Wang, X. W., Chan, C. T., Ho, K. M. & Webber, W. *Phys. Rev. Lett.* **60,** 2066–2069 (1988).
11. Fasolino, A. & Tosatti, E. *Phys. Rev.* B**35,** 4264–4283 (1987).
12. Hoffmann, F. M. *et al. Phys. Rev. Lett.* **72,** 1256–1259 (1994).
13. Peierls, R. E. *Quantum Theory of Solids* (Clarendon, Oxford, 1955).
14. Binnis, C. & Norris, C. *J. Phys.: Cond. Matt.* **3,** 5425–5436 (1991).
15. Métois, J. J. & LeLay, G. *Surf. Sci.* **133,** 422–442 (1983).
16. Huang, H., Wei, C. M., Li, H., Tonner, B. & Tong, S. Y. *Phys. Rev. Lett.* **62,** 559–562 (1989).
17. Feidenhans'l, R., Pedersen, J. S., Nielsen, M., Grey, F. & Johnson, R. L. *Surf. Sci.* **178,** 927–933 (1986).
18. Seehofer, L., Falkenberg, G. & Johnson, R. L. *Surf. Sci.* **290,** 15–25 (1993).
19. Ancilotto, F., Selloni, A. & Car, R. *Phys. Rev. Lett.* **71,** 3685–3688 (1993).
20. Crommie, M. F., Lutz, C. P. & Eigler, D. M. *Nature* **363,** 524–527 (1993).
21. Carlisle, J. A., Miller, T. & Chiang, T.-C. *Phys. Rev.* B**47,** 3790–3796 (1993), *Phys. Rev.* B**47,** 10342–10347 (1993).
22. Rice, M. J. in *Low-Dimensional Co-operative Phenomena* (ed. Keller, H. J.) 29 (Plenum, New York, 1975).
23. Carpinelli, J. M. & Weitering, H. H. *Phys. Rev.* B**53,** 12651–12654 (1996).
24. Stumpf, R. & Scheffler, M. *Phys. Rev.* B**53,** 4958–4971 (1996).
25. Overhauser, A. W. *Phys. Rev.* **128,** 1437–1452 (1962); *Phys. Rev.* **128,** 691–698 (1968).
26. Fazekas, P. & Tosatti, E. *Phil. Mag.* **39,** 229–244 (1979).
27. Han, W., Hunt, E. R., Pankratov, O. & Frindt, R. F. *Phys. Rev.* B**50,** 1476–14749 (1994).
28. Coleman, R. V. *et al. Adv. in Phys.* **37,** 559–644 (1988).

ACKNOWLEDGEMENTS. J.M.C. is on leave from the University of Pennsylvania. This research was principally supported by the National Science Foundation. We also acknowledge the support of the Petroleum Research Fund administered by the American Chemical Society, and Oak Ridge National Laboratory and Sandia National Laboratory, both managed by Lockheed Martin Energy Research Corp. for the US Department of Energy. Calculations were performed on the JRCAT-ATP supercomputer.